www.czasopisma.pan.pl PAN POLSKA AKADEMIA NAUK www.journals.pan.pl

Arch. Metall. Mater. **63** (2018), 4, 1725-1734

DOI: 10.24425/amm.2018.125098

J.G. THAKARE*#, C. PANDEY****#, R.S. MULIK*, M.M. MAHAPATRA**, H.K. NARANG***

EFFECT OF GRIT BLASTING AND THERMAL SPRAYING ON MICROSTRUCTURE EVOLUTION OF P91 WELDMENT

In the present work, studies have been carried out on the variations in the microstructure and hardness of P91 base-metal and welded joint. This variations result from the grit blasting and thermal cycle experienced during the thermal spraying process. The microstructural effects have been analyzed in terms of the depth of the deformation zone. Scanning Electron Microscopy and X-ray diffraction were used as characterization techniques. The grit blasting carried out prior to thermal spraying has resulted in the highest change in sub-surface hardness of the heat affected zone (HAZ). However, flame treatment further reduced the subsurface hardness of the heat affected zone. The depth of deformation zone was highest for inter-critical heat affected zone (IC-HAZ). The overall coating process resulted in an increase in subsurface hardness of various regions of HAZ and fusion zone (FZ). The base metal showed a 7% increase in subsurface hardness due to the overall coating process. The IC-HAZ showed maximum variation with 36% increase in subsurface hardness. The coarse grained heat affected zone (CG-HAZ) and FZ did not show any change in subsurface hardness. As a whole, the hardness and microstructure of the welded joint was observed to be more sensitive to the thermal spray coating process as compared to the base metal.

Keywords: P91, HAZ, IC-HAZ, deformation zone

1. Introduction

The efficiency of a thermal power plant predominantly depends on operating parameters. These parameters mainly include temperature, pressure and mass flow rate of steam. The upper limit for temperature and pressure is generally fixed due to material considerations. Creep strength and high-temperature oxidation behavior are properties that limit the operating temperature [1,2]. The development of Cr-Mo steels was a result of the efforts to access these elevated operating parameters. In 1974 extensive research work was carried out to develop heat resistant structural steel. The research work at Oaks Ridge National Laboratory (ORNL) led to the development of improved ferritic steel grades [3]. P91 is one of the improved steel grades which has successfully captured the power industry [4]. P91 has been successfully used at an operating temperature of 600°C [5]. Further advancement shows P92 grade being developed with the addition of boron, tungsten and reducing the weight percent of molybdenum [6]. The addition of boron enhances the creep strength of steel [7]. The microstructure of P91 steel mainly presents precipitates of metal carbides and carbo-nitrides in the ferritic matrix. Cr-Mo steels derive their strength from the stabilized M23C6 [M: Fe, Mo, Mn, Cr] type carbides precipitated along prior austenite grain boundaries (PAGBs), and stabilized MX [M: V, Nb, X: N, C] type compounds precipitated in the interior of the matrix [8-12]. Cr-Mo steels derive their strength from the stabilized M23C6 [M:Fe, Mo, Mn, Cr] type carbides precipitated along prior austenite grain boundaries (PAGBs) and stabilized MX [M: V, Nb, X: N, C] type compounds precipitated in the interior of the matrix [13,14]. Cr-Mo steels are very popular in nuclear industries due to their high creep strength and oxidation behavior. The oxidation resistance of Cr-Mo steel is lower when compared to steels with higher chromium content. On the other hand, steels with higher chromium content have lower creep strength [15]. The oxidation behavior and the service life of these alloys can be improved by suitable surface modifications. Priyantha et al. [16] successfully increased the service life of the alloy by depositing diffusion coatings containing Cr, Ni, Si and Ti etc via fluidized bed reactor chemical vapor deposition route. The coatings improved the oxidation resistance of the carbon steel substrate. The specimens exhibited corrosion properties similar to super alloys in chemical heat pump environment. Sidhu et al. [17] successfully improved the oxidation and hot corrosion behavior of T11 and T22 boiler grade steel by spraying a Ni_3Al coating. Bare metal substrate showed the least oxidation resistance where as coated samples exhibited excellent resistance to high-temperature degradation. Many researchers [18-24] have successfully used cermet and ceramic coatings to improve the performance of various substrates [25,26].

* INDIAN INSTITUTE OF TECHNOLOGY, MECHANICAL AND INDUSTRIAL ENGINEERING DEPARTMENT, ROORKEE, UTTARAKHAND 247667, INDIA.
** INDIAN INSTITUTE OF TECHNOLOGY BHUBANESWAR, SCHOOL OF MECHANICAL SCIENCE, ODISHA 751013, INDIA.
*** NATIONAL INSTITUTE OF TECHNOLOGY, RAIPUR, CHHATTISGARH 492010
**** DEPARTMENT OF MECHANICAL ENGINEERING, SRM IST DELHI NCR CAMPUS MODINAGAR UTTAR PRADESH 201204, INDIA

Corresponding authors: jayantgt88@gmail.com, chandan.py89@gmail.com

Thermal spray techniques involve applying kinetic and thermal energy to metal, alloy, ceramic or composite powder and depositing it on a substrate. The particles are heated by either controlled burning of oxygen-fuel mixtures or generating a plasma etc. The temperature of the jet during a flame spray process is in the range of 1910°C to 3150°C were as in an air plasma spray process the temperature of the plasma in the torch is in the range of 14000°C to 28000°C [27]. In a detonation gun thermal spray coating process, the hot stream of gasses can reach a temperature of 4000°C. The shock wave generated due to the detonation of fuel can reach a velocity of 3500 m/s [28]. Owing to the high temperature, Cr-Mo steels can experience microstructural changes during the coating process. The surface preparation process usually carried out prior to coating also has pronounced effect on subsurface hardness pertaining to the compressive residual stresses induced in the surface. The hardness was found to increase with increase in blasting pressure and blasting angle [29]. Momber et al. [30] studied the effect of over blasting which resulted in excessive surface hardness, reduced surface roughness and increased wettability. Owing to the extensive use of coatings on boiler tubes it becomes imperative to study the changes in mechanical and microstructural properties arising due to surface preparation and coating process.

In the present work, efforts have been made to study the effect of coating process on microstructure and hardness of both welded joint and base metal. The welded joint of Cr-Mo steel shows heterogeneity in the heat affected zone (HAZ)and is very sensitive to welding procedure and heat treatment [31,32]. Hence it becomes highly important to understand the variations in microstructure and hardness of the HAZ as a result of thermal spraying process. The commercially available Cr3C2-NiCr powder was sprayed on the substrate using detonation gun technique. The effect of grit blasting and of flame heating resulting from the coating process has been quantified in terms of variation in hardness and depth of the deformation zone.

2. Experimental

2.1. Material Processing

P91 grade boiler steel was chosen as the substrate material for the present investigation. The material was received in its as-cast and forged (C&F) condition. In as-cast and forged condition, yield strength and ultimate tensile strength were measured as 455 MPa, 655 MPa, respectively. The material was then normalized for 10 minutes at 1040°C and tempered at 760°C for 2 h as per reference [33,34]. In normalized and tempered condition, yield strength and ultimate tensile strength were measured 480 MPa, 725 MPa respectively. The normalized and tempered (NT) P91 steel was welded using gas tungsten arc welding (GTAW) process. Multi-pass welding was carried out on a V-groove with an included angle of 37.5°. The roots pass current and arc voltage conditions were 110 A and 12 V respectively. During the subsequent passes, welding current was increased to 140 A and the arc voltage was maintained at 12V. The welded joint was subjected to a post-weld heat treatment (PWHT) of 760°C for 2 h [35]. The compositional analysis of the material was carried out using an optical emission spectroscope (Metavision M-1008i). The chemical composition of P91 is given in Table 1. The surface of NT base metal and the post weld heat treated (PWHT) welded joint were subjected to grit blasting (GB), flame treatment (FT) and thermal spray coating (CD).

TABLE 1

Chemical composition of the P91 base metal in wt %

Element	C	Cr	Mn	Mo	Nb	V	N	Si	Ni	S	Cu	P	Ti
Wt %	0.10	8.5	0.54	0.95	0.05	0.20	<0.02	0.27	0.35	0.01	0.05	0.02	0.01

2.2. Surface preparation (grit blasting)

The thermal spray processes consist of substrate surface preparation, preheating of substrate and deposition of the powder. The samples with dimension 40×40×5 mm were used for thermal spray coating. Surface preparation was carried out via grit blasting before deposition to increase the roughness of the surface. The grit blasting process is a usual procedure before any thermal spray coating process. In the present work, the samples were grit blasted using alumina grit of mesh size 20 (850 microns). The samples were cleaned by directing a mixture of abrasives and high pressure compresses air on the substrate surface. Each sample was subjected to two blasting passes before coating. The process parameters associated with the grit blasting process are given in Table 2.

TABLE 2

Grit blasting process parameters

Parameter	Description	Details
1	Grit size	850 µm
2	Blasting pressure	0.30 MPa
3	No. of blasting passes	2
4	Standoff distance	150 mm
5	Blasting angle	90 degree
6	Nozzle diameter	6 mm

2.3. Thermal spray process

Thermal spray coating was done using D-gun thermal spray technique. Seven passes of coating were applied on the substrate. One of the specimens was subjected to flame treatment which did not involve any powder feed. This was carried out to study the effect of thermal cycle experienced by the substrate during coating process and is referred as flame treated (FT) sample. The coating process was carried out at SVX Powder M Surface Engineering Pvt. Ltd., Greater Noida, India. The process pa-

rameters used in the coating process are given in Table 3. After sectioning and polishing, the hardness along the cross section was measured using Vickers Hardness Tester (Omnitech-s. Auto) with 200 g load applied for 10 s. P91 steel and welded joint was coated using the same process parameters.

TABLE 3

Thermal spray process (D-gun) parameters and details

Sr.No	Process Parameter	Details
1	Working gas	Oxygen, acetylene, nitrogen, and air
2	Pressure of working gases	Oxygen 0.2 MPa, acetylene 0.14 MPa, nitrogen 0.4 MPa, air 0.4 MPa
3	Consumption of working gases	Oxygen 27×10^{-5} m^3/min, acetylene 23×10^{-5} m^3/min, nitrogen 05×10^{-4} m^3/min, and air 05×10^{-4} m^3/min
4	Consumption of powder per shot	0.05-0.02 g
5	Water consumption rate	$15\text{-}25\times10^{-3}$ m^3/ min
6	Firing rate	1-10 Hz
7	Diameter of accelerating portion of barrel or coating coverage	0.022 mm
8	Coating thickness per shot	5-25 µm
9	Power supply from main	Frequency 50-60 Hz, voltage 430 V, power 450 VA
10	Relative humidity of ambient air	50 %

2.4. Material characterization

Specimens for microstructural investigations were prepared by standard metallographic procedures. The samples were polished on various grades of emery papers. After polishing to grade 2000, samples were cloth polished using alumina powder. The samples were subsequently etched using Vilella's reagent (1g picricacid+5ml hydrochloric acid + 100 ml methanol) before SEM analysis. The subsurface hardness of GTAW welded samples was measured after heat treatment, shot blasting, flame treatment and coating deposition process. Cross-sectional analysis of the various treated samples was carried out to measure the hardness in fusion zone (FZ), heat affected zone (HAZ), base metal. The hardness was measured along the horizontal direction starting from the inter-critical heat affected zone (IC-HAZ) followed by fine grained heat affected zone (FG-HAZ), coarse grained heat affected zone (CG-HAZ) and FZ. The different regions of the heat affected zone were marked after regular metallographic practice. The through thickness hardness profile in different regions of heat affected zone was also measured. Fig. 1 shows arrow heads directed along the hardness measurement direction. Arrow heads one, two, three and four show the measurement direction for IC-HAZ, FG-HAZ, CG-HAZ and FZ respectively. The hardness of the base metal along thickness was also measured to identify the effect of the individual process on the sub-surface hardness of the sample.

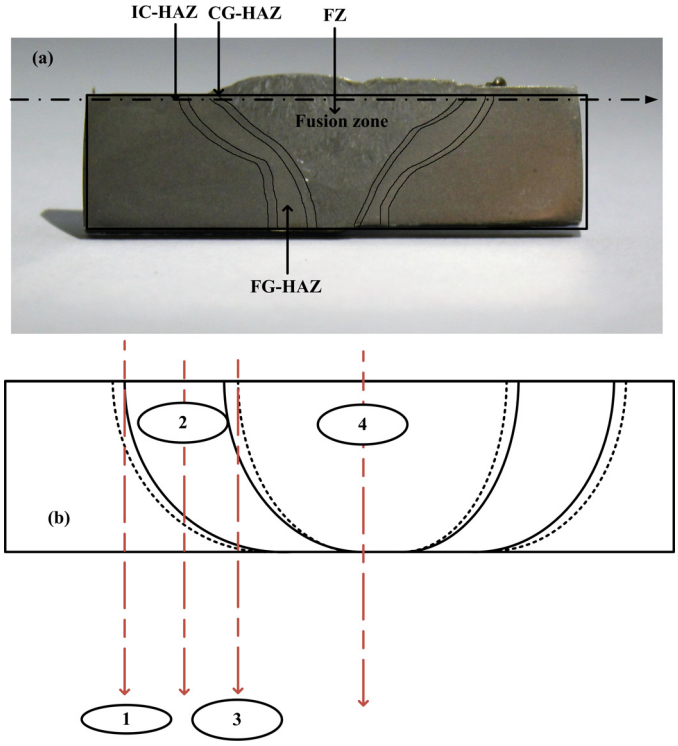

Fig. 1. (a) Macrograph showing different regions of heat affected zone and direction along which hardness profiles were taken in horizontal direction along the cross section (b) schematic showing vertical direction along which the hardness readings were taken for regions of the heat affected zone along the cross section

3. Results and discussion

3.1. Microstructure of as-received material

The steel was received in as-cast and forged condition. The microstructure in the as-received condition show tempered martensite with distinct lath blocks, as shown in Fig. 2a. The microstructure after NT shows the presence of prior austenite grain boundaries (PAGBs) and re-precipitation of dissolved precipitates as shows in Fig. 2b. The SEM micrographs shows the presence of coarse lath blocks decorated with precipitates, as shown in Fig. 3a. The PAGBs are not observed clearly in as-received condition. After the NT microstructure consists of PAGBS with lath blocks of different orientation inside the boundaries of PAGBs, as shown in Fig. 3b. The precipitates are observed in black dotted form. For detail analysis of precipitate morphology, SEM micrograph was taken, as shown in Fig. 3a,b. The larger precipitates at the PAGBs are identified to be $M_{23}C_6$ type precipitates having size in range of 100-200 nm [M:Fe,Mo,Cr] while inside the intra-lath region fine V and Nb rich carbide and carbo-nitrides type precipitates are observed with size in range of 20-40 nm [34,36,37]. P91 steel shows very high tendency to form martensite. The high chromium content promotes the formation of martensite even when the steel is subjected to very low cooling rates, as slow as 0.1 K/s [38]. During normalizing, the material is heated to a temperature above the Ac_3 (912 °C) line into single phase region (austenite) followed by air cooling. Due

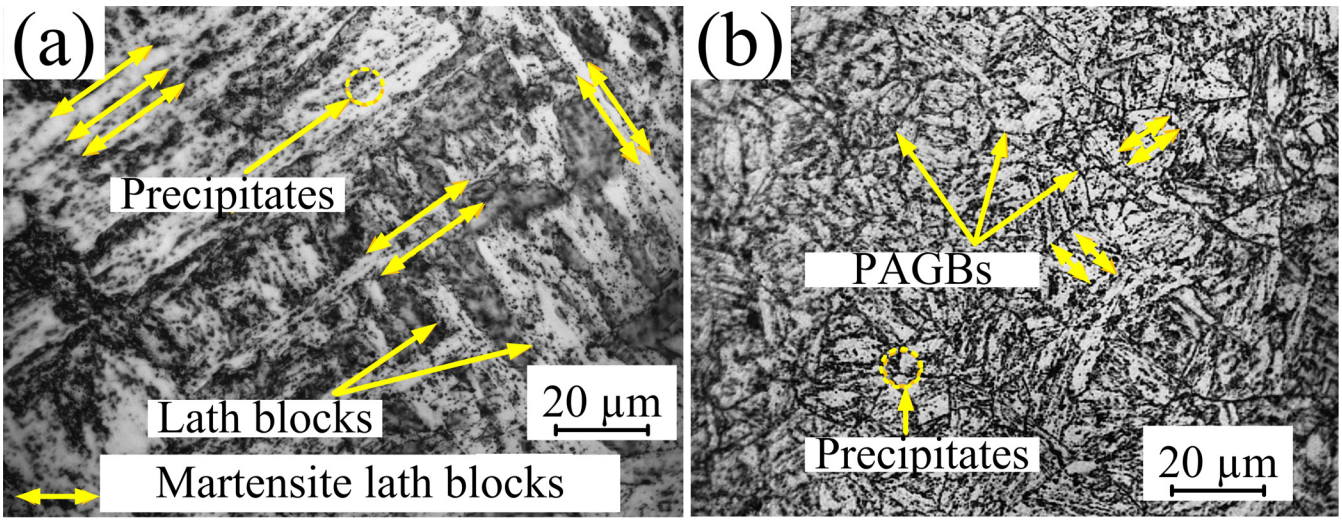

Fig. 2. (a) Optical micrograph of P91 steel in as-received condition, (b) optical micrograph of P91 steel after normalized and tempering heat treatment

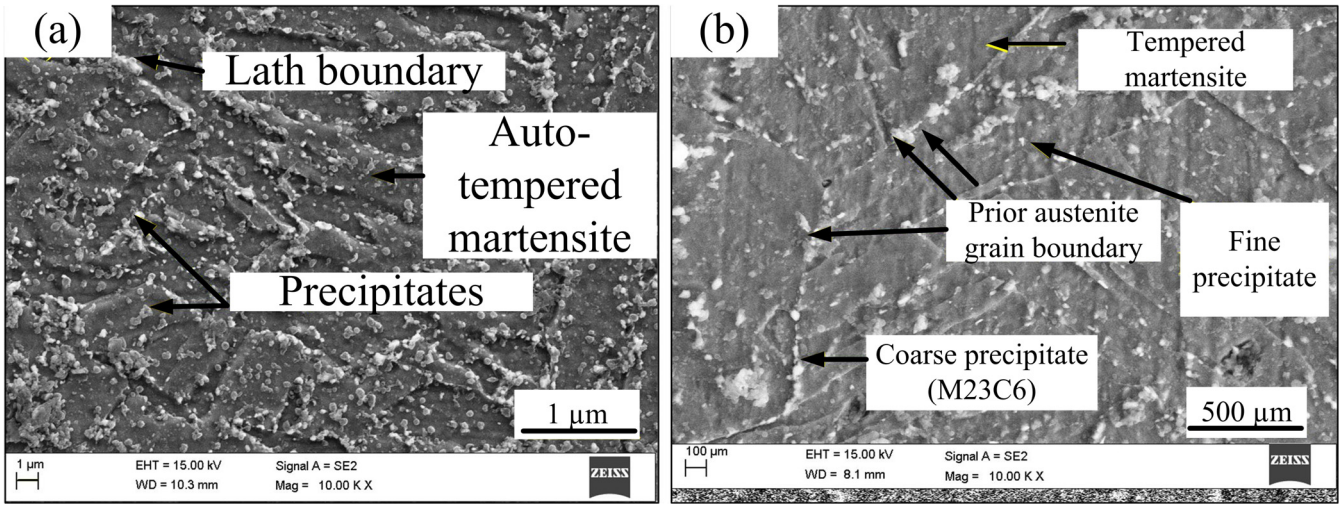

Fig. 3. (a) SEM micrograph of P91 steel in as-received (AR) condition, (b) SEM micrograph of P91 steel after normalized and tempering (NT) heat treatment

to the presence of alloying elements, even air cooling produces fresh untempered martensite. This martensite can be tempered by heating above the Ac_1 (727°C) line and cooling in air.

3.2. Microhardness of base metal

Surface preparation process has a primary influence on substrate hardness. In order to understand the influence of every sub-process, hardness profiles were taken for GB, FT, NT, and CD samples. The hardness of samples along the depth was measured and shown in Fig. 4 for different samples. The microhardness value for untreated base metal was found to be 210±5 $HV_{0.2}$, which almost remains constant with distance from the substrate surface.

Hardness along the thickness was measured on the GB, FT, NT and CD sample. The near surface hardness is notably distinct from the remaining values measured along the depth. However, beyond 0.1 mm of distance along the depth hardness did not show any steep variation over the remaining cross section of the sample. The base metal shows a hardness at 200 gm load, increase from 210 $HV_{0.2}$ to 226 $HV_{0.2}$ after GB. This increase in hardness is mainly due to strain hardening effect. Grit blasting produces a high-density dislocation network which leads to strain hardening of the surface and sub-surface. Guan et al. [39] in their work on aluminum have estimated that a depth of 100 µm was affected by sand blasting. The values measured by Vickers hardness tester suggests that the strain hardened region is within the 0.1mm distance from the surface. However, the hardness result on itself cannot provide any firm information regarding the affected depth. The affected zone was determined exactly using SEM micrographs. The size of deformation zones can be seen in the micrographs in Fig. 5a-c. The size of deformation zone is 16±4 µm for the GB sample. The FT and CD sample in Fig. 5b-c also shows the deformation zone of the same order, which implies that the effect of the powder spraying process and FT is negligible on the size of the deformation zone size.

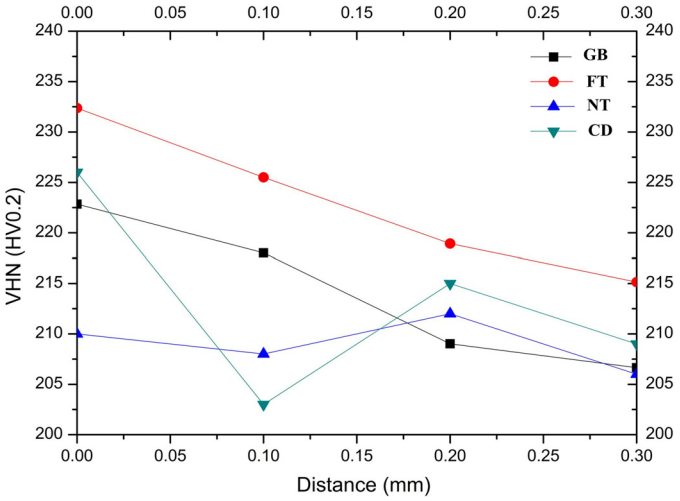

Fig. 4. Graph showing variation in hardness values along the depth for grit blasted (GB), flame treated (FT), normalized and tempered (NT) and as-coated (CD) base metal

3.3. Microhardness of welded joint

The thermal spray coating process is a result of combined heat and mass transfer. The hardness of the substrate can get affected due to both modes of energy transfer. The hardness of the heat affected zone is a very important parameter in accessing the in-service behavior of the welded joint. The hardness of P91 is affected by many factors. The primary factor responsible for increased hardness is the size and the type of precipitates. Others factors that affect the hardness include grain size, the presence of carbon and nitrogen in the matrix, dislocation density [40,41]. Hardness measurements were carried out along the cross section for all the treated samples shown in Fig. 6.

The hardness of the CG-HAZ is the highest whereas the hardness value for the region of HAZ closest to the base metal (IC-HAZ) was found to be the lowest. The IC-HAZ is critical in deciding the service behavior of the welded joint. The low

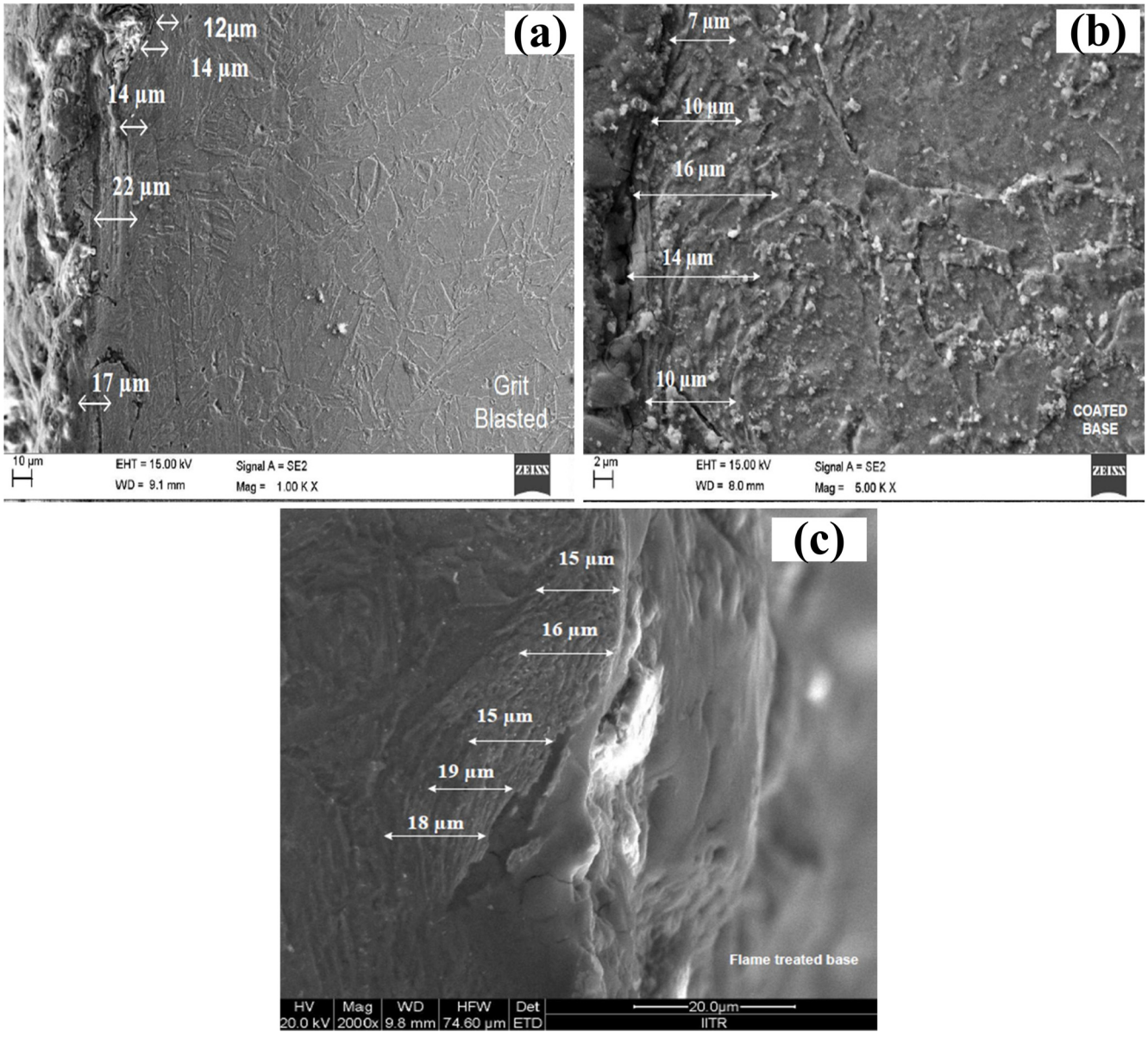

Fig. 5. SEM micrographs showing size of deformation zone in a) grit blasted P91, b) coated P91, c) flame treated P91

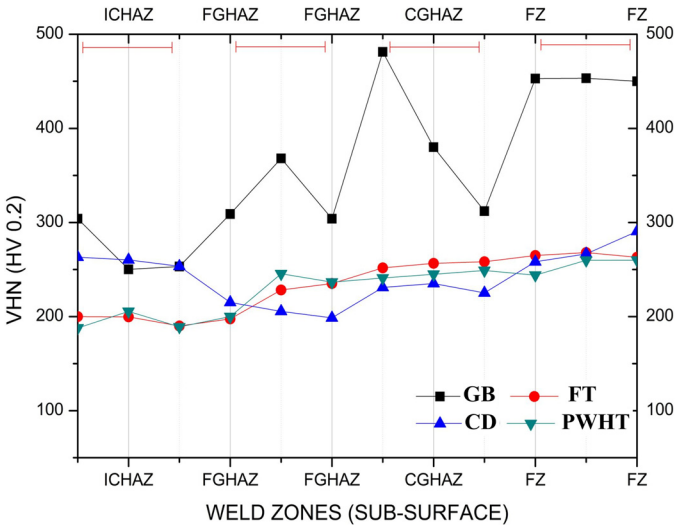

Fig. 6. Variation in hardness of post weld heat treated sample (PWHT), grit blasted weld sample (GB), flame treated weld sample (FT), coated weld sample (CD)

hardness value of the IC-HAZ makes it prone to cracking, which is called type IV cracking. The hardness readings were consistent with those available in the literature [7,31,42-44]. The average hardness in the FZ for post weld heat treated sample was found to be 250 $HV_{0.2}$. There was not much variation in the hardness reading of the CG-HAZ, which was 256 $HV_{0.2}$. The average hardness of the FG-HAZ was found to be 237 $HV_{0.2}$. The lowest hardness was noted for the IC-HAZ and was found to be 190 $HV_{0.2}$.

The IC-HAZ was found to be more sensitive to grit blasting as shown by the size of deformation zone in Fig. 7a. Grit blasting involves impinging metallic or ceramic grits against the substrate surface. The surface experiences indentation accompanied by material removal via erosion, micro-cutting, plowing etc. [45]. Micro-cutting results in material removal whereas indentation introduces compressive stress in the near-surface region of the substrate. Grit blasting introduces a deformation layer in the material which increases the dislocation density and hence

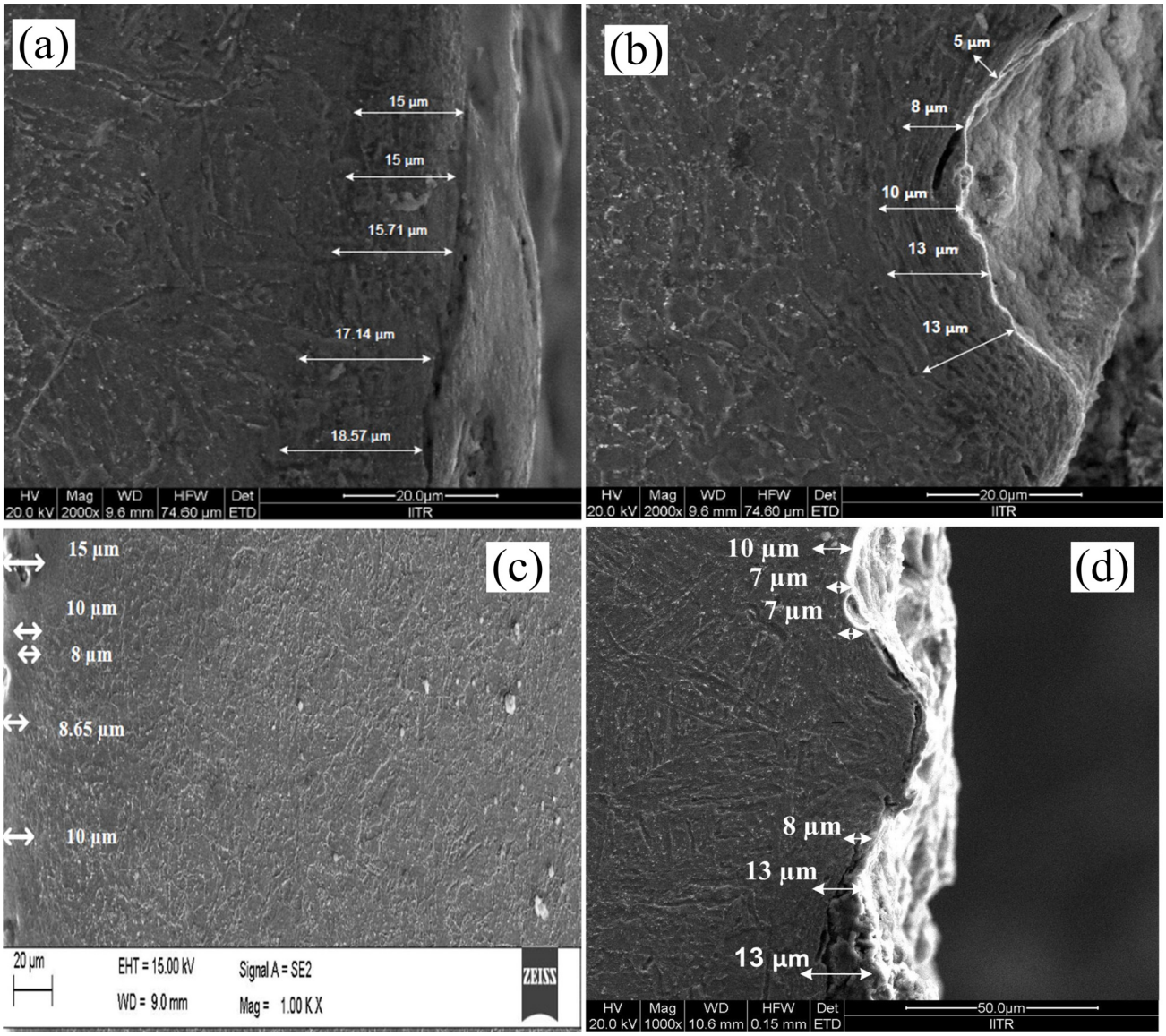

Fig. 7. SEM micrographs showing the region deformed due to grit blasting (a) inter critical heat affected zone (IC-HAZ), (b) Fine grained heat affected zone (FG-HAZ), (c) Coarse grained heat affected zone (CG-HAZ), (d) Fusion Zone (FZ)

leads to increase in hardness. However, the deformation zone is quite different from the one introduced by shot peening which mainly concentrates on improving the fatigue life by introducing compressive stresses [43]. The deformation zone can be seen in SEM images shown in Fig. 7a-d.

Its subsurface hardness increased to 320 $HV_{0.2}$ after grit blasting, exhibiting a 68% increase. The FG-HAZ showed 30% increase in its subsurface hardness value due to grit blasting, changing from 237 to 310 $HV_{0.2}$ as shown in Fig. 8b. Whereas CG-HAZ and FZ showed a 13% and 10% rise respectively and can be seen from their corresponding plot in Fig. 8c,d. The overall thermal spray coating process (Detonation Gun process) increased the IC-HAZ hardness from 190 to 260 $HV_{0.2}$. The FG-HAZ hardness increased from 237 $HV_{0.2}$ to 245 $HV_{0.2}$ as a result of the coating process. The coating process lead to 36% and 3.3% increase in subsurface hardness of IC-HAZ and FG-HAZ respectively. The CG-HAZ and fusion zone (FZ) showed negligible change in subsurface hardness after coating.

The size of deformation zone varies from region to region of the heat affected zone. The deformed zone is more or less a zone running parallel to the sample surface. The deformation zone measures around 11±4 μm, 9±3 μm in the FG-HAZ and the CG-HAZ respectively. The deformation zone measured in FZ was of the order of 10±3 μm. The deformation zone was largest in case of IC-HAZ. Fig. 7a shows a deformation zone of 16±1.5 μm in case of IC-HAZ. The depth upto which hardness is affected in the case of P91 is different for different zones of the welded joint and for the base metal.

The fine size of precipitates which are mainly responsible for the increase in hardness are also responsible for smaller size of deformation zone in CG-HAZ. During the welding process, the region closest to FZ experiences high temperature, sufficient enough to dissolve completely the precipitates that were formed during the heat treatment of the parent metal. The dissolution of precipitates leads to solid solution strengthening of CG-HAZ. The dissolved components re-precipitated after PWHT. The FG-HAZ and IC-HAZ experiences lower temperature compared to CG-HAZ; hence the fractions of precipitates that are dissolved during the weld thermal cycle are comparatively lower. The PWHT hence leads to more significant coarsening of precipitates and to less re-precipitation of particles from the matrix [46]. The resulting hardness is lower due to lower pinning effect of coarser precipitates. The fine size of precipitates might be responsible for the smaller size of deformation zone as compared to CG-HAZ. The microstructural heterogeneity and precipitate coarsening is the reason for increased deformation zone due to grit blasting.

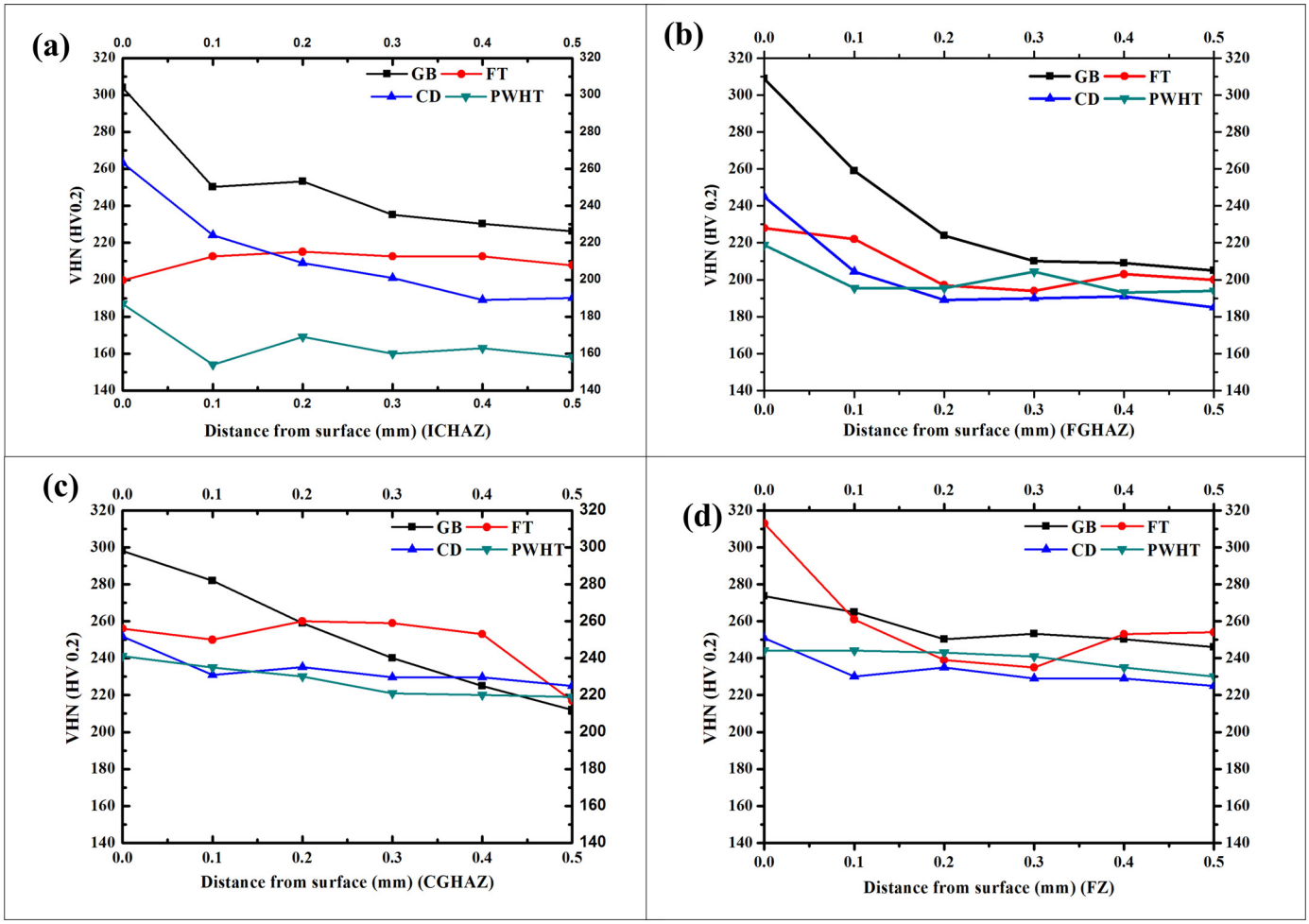

Fig. 8. Variation in hardness of different (a) inter critical HAZ (IC-HAZ), (b) fine grained HAZ (FG-HAZ), (c) coarse grained HAZ (CG-HAZ), (d) fusion zones (FZ) of post weld heat treated sample (PWHT), grit blasted weld sample (GB), flame treated weld sample (FT), coated weld sample (CD)

The region of the HAZ closest to the parent metal (IC-HAZ) experiences a peak temperature between Ac_1 and Ac_3 lines which partially transforms the matrix to austenite. During the cooling cycle, austenite transforms to fresh martensite. The thermal cycle also leads to coarsening of precipitates and reduction in number density [47]. PWHT results in a matrix comprising of both transformed and untransformed martensite. This heterogeneity is the reason for lower resistance to deformation and hence larger size of deformation zone.

Vickers hardness was also taken along the cross section of FT and CD samples. Fig. 8 shows the plot of hardness reading measured along depth for various treated samples. All regions of HAZ in the initial 0.1mm distance from the surface show a steep change in hardness after grit blasting. The flame treatment should have led to stress reliving of the deformation zone which results in reduced hardness. Fig. 9 shows the size of deformation zone for FT which is highest for IC-HAZ. This can be explained by the hardness plot after flame treatment in Fig. 8 which shows reduced subsurface hardness. IC-HAZ hardness reduced from 320 $HV_{0.2}$ to 200 $HV_{0.2}$, which further increased to 260 $HV_{0.2}$ due to powder impingement of semi-molten or solid particles during the deposition process. Larger hardness gradient over the initial 0.1mm was seen in case of FG-HAZ and IC-HAZ which is due to their lower hardness values in post weld heat treated condition. Due to lower resistance to indentation, the IC-HAZ shows the highest impact of grit blasting.

3.4. XRD analysis

Fig. 10 shows XRD spectra of variously treated base metal and welded joint. Both welded joint and base metal shows light

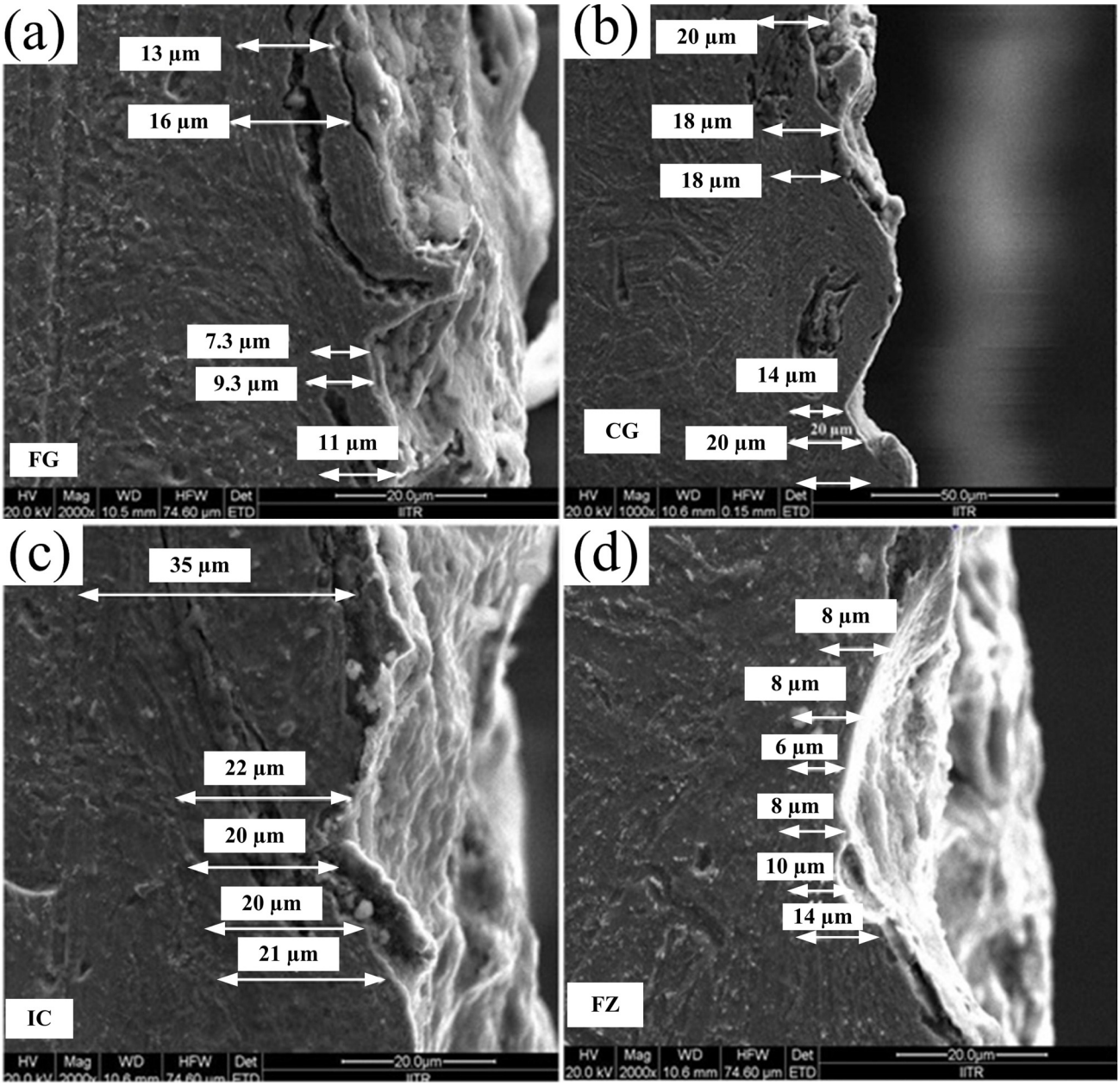

Fig. 9. SEM micrographs of flame treated weldment showing deformation zones of (a) fine grained heat affected zone (FG-HAZ), (b) coarse grained heat affected zone (CG-HAZ), (c) inter-critical heat affected zone (IC-HAZ), (d) Fusion zone (FZ)

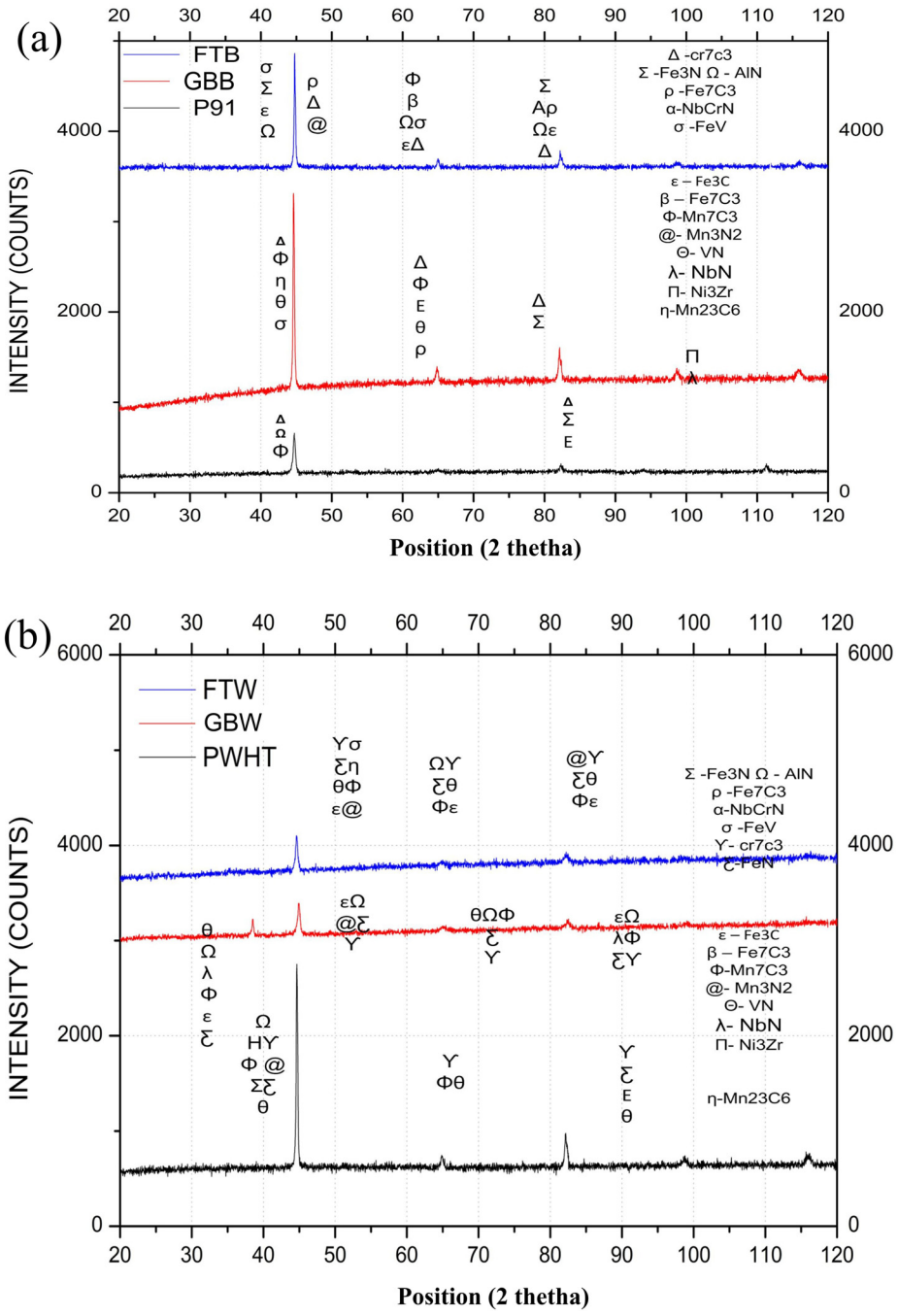

Fig. 10. XRD spectra of (a) normalized and tempered base metal (P91), grit blasted base metal (GBB), flame treated base metal (FTB), (b) post weld heat treated weld (PWHT), grit basted weld (GBW), flame treated weld (FTW)

shifting of peak due to GB and FT. The normalized and tempered sample shows peaks at position (2θ) of 44.70º, 82.31º. Grit blasting introduces plastic strain in the subsurface which shifts the peak to 2θ of 44.59º and 82.1091º. This peak shift might be due to the reduced d-spacing resulting from the blasting-induce strain. Due to straining, newer peaks have emerged at 2θ of 64.88º and 98.715º. Flame treatment of the sample further shifts the peaks near the original 2θ positions at 44.74º and 82.23º accompanied with change in d-spacing. The formation of new peaks suggests that strain induced transformation occurred due to grit blasting. No new peaks have emerged due to flame treatment which implies there was no transformation due to flame treatment. Phase transformations due to grit blasting have also been reported by Toshal et al. [43]. The XRD spectra of post weld heat treated P91 weld joint also shows similar peak shifts and generation of newer peaks. Post weld heat treated samples shows peaks at 44.61º, 64.90º, 82.13º and 98.84º. Grit blasting results in peak shifting at 44.61º, 64.90º, 82.13º to 44.921º, 65.03º and 82.48º respectively. Flame treatment shifts the peaks almost back to 2θ of 44.65º, 64.97º. New peaks are also seen at a 2θ of 38.49º referring to the strain induced deformation.

4. Conclusions

The following conclusions can be drawn from the above work.

1. The experimental results show that the effect of grit blasting and thermal spraying is primarily on subsurface hardness. A deformation zone is introduced into the material as a result of grit blasting. The size of deformation zone is highest for inter-critical heat affected zone.

2. IC-HAZ was found to be more sensitive to grit blasting exhibiting a 68% increase in subsurface hardness followed by FG-HAZ. FG-HAZ showed 30% increase in its subsurface hardness value. Whereas CG-HAZ and FZ showed a 13% and 10% rise respectively. The overall coating process leads to 36% and 3.3% increase in subsurface hardness of IC-HAZ and FG-HAZ respectively. The CG-HAZ and FZ showed negligible change in subsurface hardness

Grit blasting was primarily responsible for increase in hardness; however flame treatment and coating process also had effect on subsurface hardness but was negligible when compared to grit blasting. Flame treatment reduced the subsurface hardness resulting from grit blasting.

3. The XRD analyses show peak shift and generation of newer peaks. The shifting of the peaks is due to the changes in d-spacing of the crystal. The generation of new peaks depicts strain induced deformation in the material.

REFERENCES

[1] R. Viswanathan, J. Sarver, J.M. Tanzosh, J. Mater. Eng. Perform. **15**, 255-274 (2006). doi:10.1361/105994906X108756.

[2] C. Pandey, M.M. Mahapatra, P. Kumar, R.S. Vidyrathy, A. Srivastava, Mater. Sci. Eng. A **695**, 291-301 (2017). doi:10.1016/j.msea.2017.04.037.

[3] C. Pandey, M.M. Mahapatra, J. Mater. Eng. Perform. **25**, 2195-2210 (2016). doi:10.1007/s11665-016-2064-x.

[4] C.D. Lundin, Mater. Des. **12** (4), 193-197 (1991).

[5] S.S. Wang, D.L. Peng, L. Chang, X.D. Hui, Mater. Des. **50**, 174-180 (2013). doi:10.1016/j.matdes.2013.01.072.

[6] N. Saini, C. Pandey, M.M. Mahapatra, H.K. Narang, R.S. Mulik, P. Kumar, Eng. Fail. Anal. **81**, 245-253 (2017). doi:10.1016/j.engfailanal.2017.06.044.

[7] ASTM-A335/A335M-18a, ASTM-International, (2018). https://doi.org/10.1520/A0335_A0335M-18A

[8] M. Gwoździk, Z. Nitkiewicz, Arch. Metall. Mater. **58**, 4-31 (2013). doi:10.2478/v10172-012-0146-9.

[9] G. Golański, J. Kępa, Arch. Metall. Mater. **57**, 575-582 (2012). doi:10.2478/v10172-012-0061-0.

[10] A. Zieliński, J. Dobrzański, H. Purzyńska, G. Golański, Arch. Metall. Mater. **61**, 957-964 (2016). doi:10.1515/amm-2016-0163.

[11] G. Golański, J. Jasak, A. Zieliński, C. Kolan, M. Urzynicok, P. Wieczorek, Arch. Metall. Mater. **62**, 263-271 (2017). doi:10.1515/amm-2017-0040.

[12] I. Velkavrh, F. Kafexhiu, S. Klien, F. Ausserer, J. Voyer, A. Diem, J. Phys. Conf. Ser. **843**, 012065 (2017). doi:10.1088/1742-6596/843/1/012065.

[13] W. Yan, W. Wang, Y.Y. Shan, K. Yang, Front. Mater. Sci. **7** (1), 1-27 (2013). doi:10.1007/s11706-013-0189-5.

[14] C. Pandey, A. Giri, M.M. Mahapatra, Mater. Sci. Eng. A **664**, 58-74 (2016). doi:10.1016/j.msea.2016.03.132.

[15] M. Seraffon, A.T. Fry, D.M. Laing, Material for Advaced Power Engginering Conf. Ser. Forschungszentrum Julich, Germany (2014).

[16] N. Priyantha, P. Jayaweera, A. Sanjurjo, K. Lau, F. Lu, K. Krist. Surf. Coatings. Technol. **164**, 6-31 (2003).

[17] B.S. Sidhu, S. Prakash, Surf. Coatings. Technol. **166**, 89-100 (2003).

[18] S. Kamal, R. Jayaganthan, S. Prakash, S. Kumar, J. Alloys Compd. **463**, 358-372 (2008). doi:10.1016/j.jallcom.2007.09.019.

[19] S. Kamal, R. Jayaganthan, S. Prakash, Surf. Coatings. Technol. **203**, 1004-1013 (2009). doi:10.1016/j.surfcoat.2008.09.031.

[20] M. Suarez, S. Bellayer, M. Traisnel, W. Gonzalez, D. Chicot, J. Lesage, Surf. Coatings. Technol. **202**, 4566-4571 (2008). doi:10.1016/j.surfcoat.2008.04.043.

[21] J. Pirso, M. Viljus, S. Letunovitš, Wear, **260**, 815-824 (2006). doi:10.1016/j.wear.2005.04.006.

[22] J.F. Li, C.X. Ding, Wear **240**, 5-180 (2000). doi:10.1016/S0043-1648(00)00355-0.

[23] H.S. Sidhu, B.S. Sidhu, S. Prakash, Tribol. Int. **43**, 887-890. (2010). doi:10.1016/j.triboint.2009.12.016.

[24] B.Q. Wang, Z.R. Shui, Wear **253**, 550-557 (2002). doi:10.1016/S0043-1648(02)00049-2.

[25] J.G. Thakare, C. Pandey, RS. Mulik, M.M. Mahapatra. Ceram. Int. **44**, 6980-6989 (2018). doi:10.1016/j.ceramint.2018.01.131.

[26] J.G. Thakare, R.S. Mulik, M.M. Mahapatra. Ceram. Int. **44**, 438-451 (2018). doi:10.1016/j.ceramics int.2017.09.196.

[27] J.R. Davis, Handbook of Thermal Spray Technology, ASM International (2004).

[28] L. Singh, V. Chawla, J.S. Grewal, J. Miner. Mater. Charact. Eng. **11**, 243-265 (2012).

[29] K.C. Poorna, M. Vashista, K. Sabiruddin, S. Paul, P.P. Bandyopadhyay, Mater. Des. **30**, 2895-2902 (2009). doi:10.1016/j.matdes.2009.01.014.

[30] A.W. Momber, Y.C. Wong, JCT Res. **61002E**, 2:453 (2005)

[31] C. Pandey, M.M. Mahapatra, J. Mater. Eng. Perform. **25**, 2761-2775 (2016). doi:10.1007/s11665-016-2127-z.

[32] A.K. Singh, M. Kumar, V. Dey, R.N. Rai, IOP conf. Ser. Mater. Sci. Eng. **225**, 012099 (2017).

[33] C. Pandey, A. Giri, M.M. Mahapatra, Materials Science & Engineering A **657**, 173-84 (2016). doi:10.1016/j.msea.2016.01.066.

[34] C. Pandey, M.M. Mahapatra, P. Kumar, N. Saini, Trans. Indian. Inst. Met. **4**, 1-20 (2017). doi:10.1007/s12666-017-1144-4.

[35] C. Pandey, M.M. Mahapatra, P. Kumar, A. Giri. Met. Mater. Int. **23**, 900-14 (2017). doi:10.1007/s12540-017-6850-2.

[36] C. Pandey, N. Saini, M.M. Mahapatra, P. Kumar, Int. J. Hydrogen Energy **41**, 17695-17712 (2016). doi:10.1016/j.ijhydene.2016.07.202.

[37] C.G. Panait, W. Bendick,A. Fuchsmann, A.F.G. Lorenzon, J. Besson, Int. J. Press Vessel. Pip. **87**, 326-35 (2010). doi:10.1016/j.ijpvp.2010.03.017.

[38] P. Parameswaran, S. Saroja, M. Vijayalakshmi, J. Nucl. Mater. **232**, 226-232 (1996).

[39] X.S. Guan, Z.F. Dong, D.Y. Li, Nanotechnology **16**, 2963-2971 (2005). doi:10.1088/0957-4484/16/12/040.

[40] C. Pandey, M.M. Mahapatra, Trans Indian Inst Met **69**, 1657-1673 (2016). doi:10.1007/s12666-015-0826-z.

[41] C. Pandey, M.M. Mahapatra, P. Kumar, N. Saini, Mater. Sci. Eng. A **712**, 720-37 (2018). doi:10.1016/j.msea.2017.12.039.

[42] S. Sulaiman, Structure of properties of the heat affected zone of P91 creep resistant steel, PhD thesis, University of Wollongong, New South Wales, Australia, 2007.

[43] K. Toshal, J. Lu, B. Guelorget, E. Nagashima, ICSP9 400-405 (2001).

[44] C. Pandey, M.M. Mahapatra, P. Kumar, N. Saini, J.G. Thakre, R.S. Vidyarthy, Arch. Civ. Mech. Eng. **18**, 713-22 (2018). doi:http://dx.doi.org/10.1016.

[45] P. Valášek, M. Müller, Manuf. Technol. **16**, 1371-1380 (2016).

[46] N. Gutiérrez, J. Alvarado, H. Cicco, A. Danón. Procedia Mat. Sci. **8**, 1140-1149 (2015). doi:10.1016/j.mspro.2015.04.178.

[47] A. Moitra, P. Parameswaran, P.R. Sreenivasan, S.L. Mannan. Mater. Charact. **48**, 55-61 (2002). doi: 10.1016/S1044-5803(02)00247-4